

# Evaluation of Hessian-based filters to enhance the axis of coronary arteries in CT images

S.D. Olabarriaga <sup>a,\*</sup> M. Breeuwer <sup>b</sup> W.J. Niessen <sup>a</sup>

<sup>a</sup>*University Medical Center Utrecht, Image Sciences Institute,  
Heidelberglaan 100, 3584 CX Utrecht, NL*

<sup>b</sup>*Philips Medical Systems, Medical IT - Advanced Development,  
Building QV 162, P.O. Box 10000, 5680 DA Best, NL*

---

## Abstract

This work describes an evaluation of three Hessian-based filters for enhancement of the central axis of coronary arteries in multi-detector CT images acquired with contrast injection. These filters analyze the main modes of second-order variation in image intensity to determine the type of local structure present in the image (tubular-like). The average filter response obtained with different parameter configurations was measured at fixed distances from a reference central axis determined manually. Results were compared with two objective measures, namely the response decay rate at the center and the overall response within 5 mm.

*Key words:* coronary arteries, vessel axis, cardiac CT, enhancement, evaluation

---

## 1 Introduction

Developments in multi-detector CT and reconstruction techniques allow for fast acquisition of high-resolution images, with large impact on cardiac imaging. Images acquired with contrast injection (CMDCT) contain much detail of the complex heart structure, with promising perspectives for assessment of coronary artery disease in a less invasive manner than conventional angiography.

The analysis of such images requires digital post-processing to isolate the coronary arteries from the complex background. Several methods for vessel enhancement and segmentation are based on the knowledge that vessels are

---

\* Corresponding author (*silvia@isi.uu.nl*).

tubular structures that could be described by their central axes and width. Some methods for central vessel axis (CVA) segmentation (e.g., [1], [2]) extract information from  $2^{nd}$ -order derivatives at multiple scales to identify the type of local structure present in the image (e.g. tubular-like) by inspecting the main modes of variation in the Hessian matrix. Hessian-based vessel enhancement filters (HBVF) have been proposed by Lorenz et al. [3], Sato et al. [4], and Frangi et al. [5]. These have been shown to be applicable to various imaging modalities (e.g., DSA [3,5], CTA [4] and 3-D MRA [5,4,1]) and several types of vessels (cerebral [3,4], peripheral [5], hepatic [4], pulmonary [4], cardiac [1]). In this work we investigate and compare their capabilities to enhance the coronary artery *axis* in CMDCT images.

## 2 Materials and Methods

**Filters.** In a multi-scale framework, a HBVF is defined as  $F(\mathbf{x}) = \max_{\sigma} f(\mathbf{x}, \sigma)$ , where  $\mathbf{x}$  is a position in the image,  $f$  is the filter, and  $\sigma$  is the scale for calculating Gaussian image derivatives. In this study, the filter response is calculated for 10 exponentially-distributed scales in the interval [0.5, 5] mm. The filters calculate  $2^{nd}$ -order derivatives, build the Hessian matrix  $\mathcal{H}$ , decompose it into eigenvalues  $\lambda_1$ ,  $\lambda_2$  and  $\lambda_3$ , and analyze them to determine the likelihood of  $\mathbf{x}$  belonging to a vessel. This analysis is based on the following hypotheses (for bright vessels, dark background,  $|\lambda_1| < |\lambda_2| < |\lambda_3|$ ): (a)  $\lambda_1 \approx 0$  corresponds to the eigenvector tangent to the CVA; (b)  $\lambda_2 \approx \lambda_3 < 0$ ; and (c)  $|\lambda_1| \ll |\lambda_2|$ . The filters differ in how they test the hypotheses and generate a quantity indicating vessel-likelihood. In all cases,  $f(\mathbf{x}, \sigma) = 0$  if  $\lambda_2 > 0$  or  $\lambda_3 > 0$ .

The filter defined by Lorenz et al. [3] was implemented as:

$$\mathcal{L}(\mathbf{x}) = \sigma^{\eta} \left| \frac{\lambda_2 + \lambda_3}{2.0} \right|, \quad (1)$$

where  $\eta$  normalizes responses across scales.

The filter defined by Sato et al. in [4] was implemented as follows:

$$\mathcal{S}(\mathbf{x}) = \begin{cases} \sigma^2 |\lambda_3| \left( \frac{\lambda_2}{\lambda_3} \right)^{\xi} \left( 1 + \frac{\lambda_1}{|\lambda_2|} \right)^{\tau}, & \lambda_3 < \lambda_2 < \lambda_1 < 0 \\ \sigma^2 |\lambda_3| \left( \frac{\lambda_2}{\lambda_3} \right)^{\xi} \left( 1 - \rho \frac{\lambda_1}{|\lambda_2|} \right)^{\tau}, & \lambda_3 < \lambda_2 < 0 < \lambda_1 < \frac{|\lambda_2|}{\rho} \end{cases} \quad (2)$$

where  $\xi \geq 0$  controls cross-section asymmetry,  $\tau \geq 0$  controls the sensitivity to blob-like structures,  $0 < \rho \leq 1.0$  controls sensitivity to the vessel curvature, and  $\sigma^2$  normalizes responses across scales.

The filter defined by Frangi et al. in [5] was implemented as follows:

$$\mathcal{F}(\mathbf{x}) = \left( 1 - e^{-\frac{A^2}{2\alpha^2}} \right) e^{-\frac{B^2}{2\beta^2}} \left( 1 - e^{-\frac{S^2}{2\gamma^2}} \right) \quad (3)$$

where  $A = \frac{|\lambda_2|}{|\lambda_3|}$  (controlled by  $\alpha$ ) discriminates plate- from line-like structures;  $B = \frac{|\lambda_1|}{\sqrt{|\lambda_2\lambda_3|}}$  (controlled by  $\beta$ ) discriminates from blob-like structures and  $S = \sqrt{\lambda_1^2 + \lambda_2^2 + \lambda_3^2}$  (controlled by  $\gamma$ ) eliminates background noise. Scale normalization is achieved by multiplying  $\mathcal{H}$  by  $\sigma^2$  before eigenvalue decomposition.

**Evaluation.** Fourteen coronary artery segments (CAS) in 5 CMDCT images acquired with 4-detector Philips CT scanners at different sites were used (spacing: in-plane  $\in [0.4, 0.55]$  mm, slice  $\in [0.6, 1.3]$  mm). The images were resampled to obtain isotropic voxels. The CVA of 14 CAS, with lengths  $\in [30, 100]$  mm, were traced manually by one operator using the Path Tracking Tool of the Philips EasyVision workstation. The axes were exported as curves  $p(t)$ , where  $t$  is position on the path (in mm), and adopted as reference to generate a “straightened” vessel representation used for evaluation. At each  $t$ , the tangent  $p'(t)$  to the curve determines the normal vector to the cross-sectional plane (see Fig. 1-left) spanned by the vectors  $\vec{v}$  and  $\vec{u}$ . Vectors are determined as follows for angular continuity between cross sections at  $t_i$  and  $t_{i-1}$  (see [6]):

$$\vec{n} = \frac{p'(t)}{\|p'(t)\|}, \quad \vec{u}(t_i) = \frac{\vec{u}(t_{i-1}) - \vec{n}(t_i) (\vec{u}(t_{i-1}) \cdot \vec{n}(t_i))}{\|\vec{u}(t_{i-1}) - \vec{n}(t_i) (\vec{u}(t_{i-1}) \cdot \vec{n}(t_i))\|}, \quad \vec{v} = \vec{u} \times \vec{n}.$$

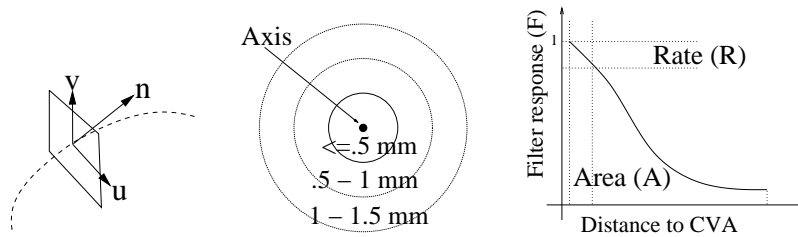


Fig. 1. Left: Cross-sectional plane vectors. Center: Concentric regions for response analysis. Right: Curve used for HBVF evaluation (normalized filter response vs. distance to the axis), and the objective measures (decrease rate and area under the curve).

The straightened vessel representation consists of a pile of vessel cross sections obtained with trilinear interpolation (spacing: path=0.3 mm, in-plane=0.2 mm). This representation is used to calculate the *mean* filter response at concentric and equally spaced regions around the CVA (Fig. 1-center), and to generate curves such as illustrated in Fig. 1-right. Two objective measures are extracted from the normalized curves to compare the response of different HBVF configurations: the decrease rate of response near the CVA ( $R$ ) and the area under the curve ( $A$ ). The measure  $R$  corresponds to the curve slope at 0.5 mm from the CVA. Small values of  $A$  and large values of  $R$  are preferred for CVA enhancement.

### 3 Results

**Lorenz filter.** The value of  $\eta$  in Eq.(1) was varied in  $[0, 4]$  at steps of  $\approx 0.25$ ; see mean results obtained for 14 CAS in Fig. 2. In the majority of cases (10 CAS), the two criteria (area and rate) point to  $\eta = 0$  as the optimal configuration. This in practice means that no scale normalization took place and the maximum filter response was obtained at small  $\sigma$  (0.5 to 0.8 mm). In other words, the structures actually “detected” by the filter are thinner than the actual coronary arteries, which should not be a problem for *axis* enhancement. Only in two cases, with large vessel width variation, better results were obtained with  $\eta \approx 1.5$ .

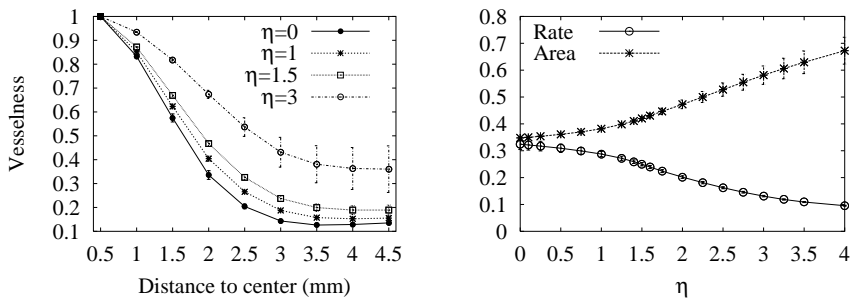


Fig. 2. Lorenz filter: normalized responses (left) and objective measures (right).

**Sato Filter.** The value of  $\rho$ ,  $\tau$ , and  $\xi$  in Eq.(2) were independently varied in the range  $[0, 1]$ , with steps of 0.1. The values assumed by the fixed parameters were  $\rho = 0.1$ ,  $\tau = 0.25$ , and  $\xi = 0.25$ . Results are quite insensitive to  $\rho$ , with very small differences between the best and worst cases, although  $\rho = 1$  is pointed out as the optimal value for all images. For variation in  $\tau$ , the difference between results is insignificant ( $\leq 0.01$  for area and rate), and no preferred optimal value could be found. The influence of  $\xi$  seems to be predominant, indicating that optimal results are obtained when  $\xi = 1$  in most cases (12 CAS) – see Fig. 3.

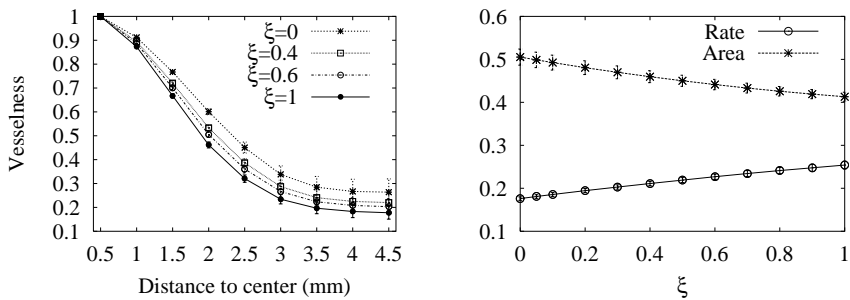


Fig. 3. Sato filter: responses (left) and objective measures (right) for varying  $\xi$ .

**Frangi Filter.** Each parameter in Eq.(3) was varied independently in the following ranges:  $\alpha \in [0, 1]$ ,  $\beta \in [0.1, 1]$  and  $\gamma \in [1, 500]$ . The values assumed

by the fixed parameters were  $\alpha = 0.4$ ,  $\beta = 0.6$  and  $\gamma = 200$ . The objective measures obtained from mean results for 14 CAS are presented in Fig. 4. For the large majority of cases (11 CAS), the best results are obtained for  $\alpha = 1$  and  $\beta = 0.1$ , although the filter response is quite insensitive to these parameters. The parameter  $\gamma$  seems to dominate the filter outcome, with optimal performance obtained when  $\gamma \geq 100$  in most cases (10 CAS).

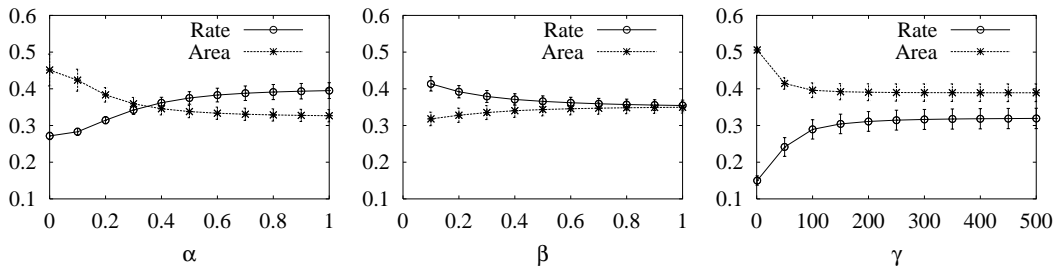


Fig. 4. Frangi filter: objective measures for varying  $\alpha$  (left),  $\beta$  (center), and  $\gamma$  (right).

#### 4 Discussion and Conclusions

From the results presented in Section 3, we chose the following parameter configurations to obtain good CVA enhancement in the average of all CAS evaluated in this study: Lorenz, Eq.(1):  $\gamma = 0$ ; Sato, Eq.(2):  $\alpha = 1$ ,  $\beta = 0.5$ ,  $\gamma = 1$ ; Frangi, Eq.(3):  $\alpha = 1$ ,  $\beta = 0.1$ ,  $\gamma = 100$ . Figure 5 shows mean results for 14 CAS obtained with the “optimal” configuration of each filter. Note that the Frangi filter provides better CVA enhancement in general (11 and 13 CAS respectively for rate or area measures). Since the response of this filter is largely dominated by the background noise suppression term (parameter  $\gamma$  in Eq.(3)), we conclude that, in the case of the images considered in this study, this is an important factor to be taken into account for CVA enhancement, besides the relationships among eigenvalues.

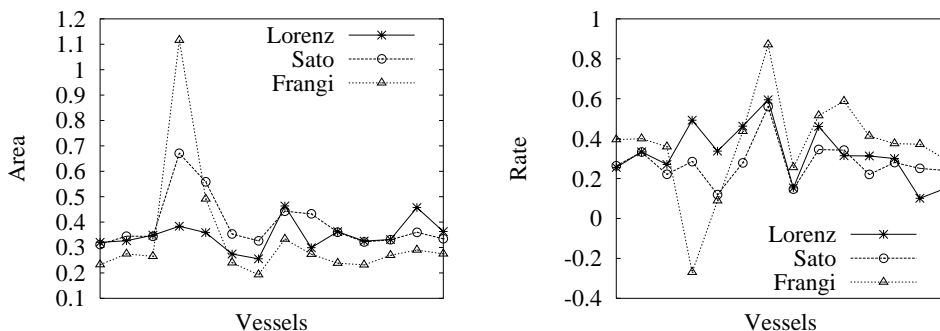


Fig. 5. Results for all filters with the optimal parameter configuration (see text). Left: Area. Right: Rate.

The results obtained with this study show that the hypotheses about relationships among the eigenvalues of the Hessian matrix (Section 2) influence the filter response differently for CVA enhancement. The hypothesis (b) is built into all filters as a test, and explicitly as a ratio in Sato and Frangi. This term seems to be important, given its weight in the optimal configuration determined experimentally ( $\xi = 1$  for Sato,  $\alpha = 1$  for Frangi). The hypothesis (c) is incorporated into the Sato and Frangi filters as a ratio between  $\lambda_1$  and the other eigenvalues. This term, however, does not seem to have an important role, since the filter response is quite insensitive to  $\tau$  and  $\beta$ , which control the term's weight respectively in Eq.(2) and Eq.(3). The hypothesis (a) is partially incorporated into the Sato filter, but it does not seem to influence the result in the optimal configuration ( $\rho = 1$  in Eq.(2)).

To conclude, note that the objective measures adopted in this study can only capture the average filter behaviour near the CVA. Other aspects could be investigated for a more thorough evaluation, such as the amount of false positive responses far from the CVA, or the behaviour at special cases such as stenosis, plaque and calcifications. This is the target of our current research.

**Acknowledgements.** We are grateful to the following institutions for providing the data for this study: Univ. Hosp. Cleveland (USA), Klinik Mue-Pasing (Prof. Haberl, Germany), Rad. Klinik Univ. Bonn (Germany) and Diagnostico Maipu. This research is funded by Philips Medical Systems, Medical IT - Advanced Development, Best (NL).

## References

- [1] O. Wink et al.: 3D MRA Coronary Axis Determination using a Minimum Cost Approach. *Magnetic Resonance in Medicine* 2002;47(6):1169:1175.
- [2] S.R. Aylward and E. Bullit: Initialization, Noise, Singularities, and Scale in Height Ridge Traversal for Tubular Object Centerline Extraction. *IEEE Trans. on Medical Imaging* 2002;21(2):61-75.
- [3] C. Lorenz et al.: Multi-scale Line Segmentation with Automatic Estimation of Width, Contrast and Tangential Direction in 2D and 3D Medical Images. In *CRVMed-MRCAS Proceedings*. Springer Verlag, 1997. p. 233-242
- [4] Y. Sato et al.: 3-D Multi-Scale Line Filter for Segmentation and Visualization of Curvilinear Structures in Medical Images. *Medical Image Analysis* 1998;2(2):143-168.
- [5] A.F. Frangi et al.: Multiscale Vessel Enhancement Filtering. In: *MICCAI Proceedings*. Springer Verlag, 1998. p.130-137.
- [6] P.J. Yim et al.: Vessel Surface Reconstruction with a Tubular Deformable Model. *IEEE Trans. on Medical Imaging* 2001;20(12):1411-1421.